Impurity transport with a transport barrier in 5D gyrokinetic simulations

G. Lo-Cascio[1], E. Gravier[1], T. Réveillé[1], M. Lesur[1], X. Garbet[2,3],Y. Sarazin[2],
K. Lim[4], G. Dif-Pradalier[2], P. Donnel[2], A. Guillevic[1], T. Rouyer[1], V. Grandgirard[2]

[1] *IJL, UMR 7198 CNRS, Université de Lorraine, 54000 Nancy, France*

[2] *CEA, IRFM, F-13108 Saint-Paul-lez-Durance, France*

[3] *School of Physical and Mathematical Sciences, Nanyang Technological University, 637371 Singapore*

[4] *Ecole Polytechnique Fédérale de Lausanne (EPFL), Swiss Plasma Center, EPFL SB SPC, Station 13, CH-1015 Lausanne, Switzerland*

Impurity transport in tokamaks is a complex process that is governed by turbulent and collisional (i.e. neoclassical) transport. Heavy impurities, such as tungsten, are known to be accumulated in the core region of tokamaks mainly due to the inward neoclassical convection [1]. The impact of a transport barrier on this transport is studied using 5D gyrokinetic GYSELA [2] simulations in presence of ITG turbulence [3]. Such a transport barrier is triggered and maintained by a strongly sheared $E \times B$ poloidal flow driven by an external poloidal momentum source (i.e. vorticity) [4] that locally polarizes the plasma. It results in a locally reduced turbulent heat diffusivity coefficient and a slight increase in core pressure as compared to the case without transport barrier [5].

Model and source term

Both the Vlasov and quasi-electroneutrality equations are coupled in GYSELA in a self-consistent model. Adiabatic electrons are chosen and the following equations are solved for the different ion species present in the plasma (i.e. Deuterium and impurities):

$$B^{\star}_{\parallel,s}\partial_t \bar{F}_s + \nabla\cdot\left(\dot{\mathbf{x}}_{GC,s}B^{\star}_{\parallel,s}\bar{F}_s\right) + \partial_{v_{G\parallel,s}}\left(\dot{v}_{G\parallel,s}B^{\star}_{\parallel,s}\bar{F}_s\right) = \mathscr{C}\left(\bar{F}_s\right) + \mathscr{S}\left(\bar{F}_s\right), \tag{1}$$

$$en_{e_0}\left(\frac{\phi - \langle\phi\rangle_{FS}}{T_e}\right) - \sum_s Z_s\nabla_\perp\cdot\left(\frac{n_{0,s}}{B_0\omega_{c,s}}\nabla_\perp\phi\right) = \sum_s Z_s\int dv_s\,\mathscr{J}\left[\bar{F}_s - \bar{F}_{eq,s}\right], \tag{2}$$

where $\bar{F}_s$ is the species gyro-center distribution function, ϕ the electrostatic potential, $\mathbf{x}_{GC,s}$ and $v_{G\parallel,s}$ the gyro-center position and parallel velocity respectively. The gyro-average and collision operators are represented by $\mathscr{J}$ and $\mathscr{C}\left(\bar{F}_s\right)$ respectively, with collisions conserving both energy and particles and taking into account both *intra* and *inter* species collisions. $\langle\ldots\rangle_{FS} = \iint\ldots J_\chi d\theta d\varphi / \iint J_\chi d\theta d\varphi$ represents the flux-surface average operation with $J_\chi = (\mathbf{B}\cdot\nabla\theta)^{-1}$ the flux-surface jacobian. $\mathscr{S}$ are the source terms, like the heat and vorticity sources. Once gyro-averaged and integrated over the phase-space, equation (1) gives the fluid vorticity conservation equation:

$$\partial_t W + \partial_r \mathscr{K} = S_0 \nabla_\perp^2 S_r \tag{3}$$

with $\mathscr{K} = e\left\langle \int dv^\star \mathscr{J}\left[(d_t \mathbf{x}_G \cdot \nabla r)\bar{F}\right]\right\rangle_{FS}$ the fluid vorticity flux, $W = e\left\langle \int dv \mathscr{J}\left[\bar{F}\right]\right\rangle_{FS}$ the fluid vorticity and $S_0\nabla_\perp^2 S_r$ the fluid vorticity source term. S_0^Ω and $S_r^\Omega(r)$ are respectively the source amplitude and radial profile of the vorticity source.

Transport barrier setup

A scrape-off layer-like (SOL-like) operator has been implemented in GYSELA to relax the electrostatic potential ϕ towards the pre-sheath conditions which requires the choice of a specific initial radial density profile with a steeper gradient at the separatrix ($r/a = 1$) as shown in Figure 1a. Heat and vorticity source profiles are shown in Figure 1b. Figure 2a shows that when $\omega_{E\times B}$ reaches a value close to $\bar{\gamma}_{lin}$, the turbulent heat diffusivity is quenched. Final temperature profiles show steeper gradients and higher core temperatures in the vorticity case as shown in figure 2b. Energy confinement is therefore enhanced; these observations confirm that the transport barrier was well triggered. We then let both the reference and vorticity simulations reach a time of $t = 220000\omega_{c,i}^{-1}$ where they converge to a quasi steady-state with almost constant pressure radial profiles.

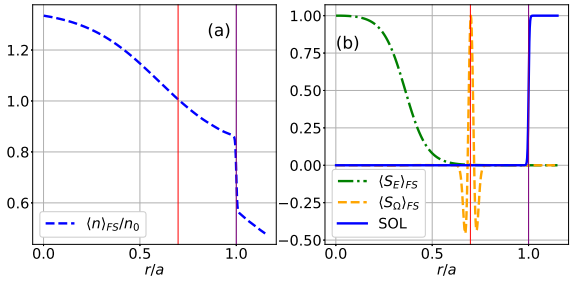

Figure 1: ***(a):*** *Initial density radial profile.* ***(b):*** *Normalized radial profiles of the axisymmetrical SOL mask (solid blue line), fluid energy source (dotted green line) and fluid vorticity source (dashed orange line). The purple vertical line indicates the separatrix position while the red one indicates the vorticity source location if activated.*

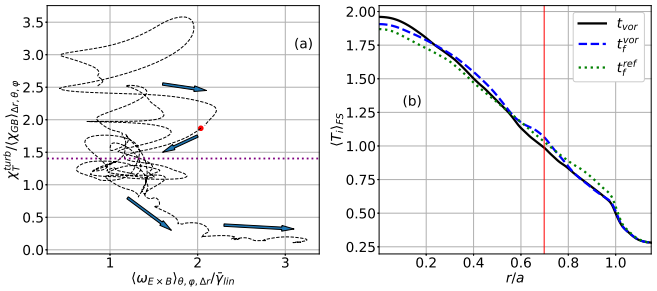

Figure 2: ***(a):*** χ_T^{turb} *against* $\omega_{E\times B}$ *at* $r/a = [0.65, 0.75]$. *The red dot represents the vorticity activation time for the vorticity case* $t_{vor}\omega_{c,0} = 100000$. *Arrows indicate the time evolution. The dotted horizontal line represents half of the average value of* $\chi_T^{turb}/\langle\chi_{GB}\rangle_{\Delta r,\theta,\varphi}$ *prior to the source activation.* ***(b):*** *Initial temperature profile (*t_{vor}*, solid black line) and fianl time of the reference (*t_f^{ref}*, dotted green line) and vorticity (*t_f^{vor}*, dashed blue line) cases.*

Impurity transport

We run a first simulation with the main ion species only (i.e. D^+, no impurities) for a sufficiently long time to reach the steady state. Once reached, we inject impurities at $t_{imp} = 220000\omega_{c,i}^{-1}$ for another run for $50000\omega_{c,i}^{-1}$. Impurity particle fluxes can be separated in two channels

$$\Gamma^{neo} = \left\langle \int \left(v_D^r + v_{E_{n=0}}^r\right) \bar{F}_s dv \right\rangle_{FS}, \tag{4}$$

$$\Gamma^{turb} = \left\langle \int v_{E_{n\neq 0}}^r \bar{F}_s dv \right\rangle_{FS}, \tag{5}$$

where Γ^{neo} and Γ^{turb} are the flux-surfaced averaged neoclassical and turbulent particle fluxes respectively. $\mathscr{E} = \mu B + \frac{1}{2} v_{G\|}^2$, $v_D^r = \bar{\mathbf{v}}_D \cdot \nabla r$ and $v_E^r = \bar{\mathbf{v}}_{E\times B} \cdot \nabla r$ are respectively the curvature plus B gradient and $E \times B$ drift velocities projected alond the radial axis. The neoclassical channel is the sum of the curvature and gradient drift contributions as well as the toroidally axisymmetric $E \times B$ drift contribution while the turbulent channel is the non toroidally axisymmetric $E \times B$ drift contribution. The total flux-surfaced averaged particle flux can then be written as $\Gamma^{tot} = \Gamma^{turb} + \Gamma^{neo}$. Since we are interested in the dynamics near the source (i.e. $r/a = 0.7 \pm 0.05$) and the core ($r/a \leq 0.65$), we choose to focus on a radial region going from $r/a = 0$ to $r/a = 0.9$ since particle flux is affected by the boundary conditions after $r/a = 0.9$.

Figure 3 shows that helium transport changes sign when the transport barrier is present as opposed to the reference case. Helium then accumulates toward the core instead of being flushed outward. Interestingly, argon and tungsten transport profiles do not change much for $r/a \leq 0.5$. However, a sheared layer of transport appear for all species with a strong negative flux inside the transport barrier and a positive one outside.

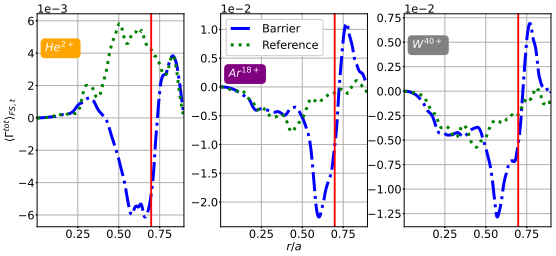

Figure 3: *Total particle flux-surface averaged fluxes for helium (left), argon (center) and tungsten (right) in the reference (dotted green lines) and vorticity (dotted-dashed blue lines) cases. All profiles are time averaged over the last* $5000\omega_{c,i}^{-1}$ *of the simulations.*

To understand this transport, theoretical neoclassical fluxes based on theory [6, 7] are used as they showed a great agreement with GYSELA results. Figure 4 shows that for helium, which is in a low collisionality regime, the Banana-Plateau (BP) terms dominate in the reference case. Both argon and tungsten fluxes in the reference case show that the Pfirsch-Schlüter component becomes important for $r/a > 0.6$. However, when the transport barrier is present, the BP flux becomes important in the source region with the characteristic sheared profile observed previously for all species. This is due to the poloidally asymmetric nature of the source which injects pressure anisotropy. The term $\Gamma^{\Pi_\|} = -\frac{I}{Ze}\left\langle \frac{B^2}{N_z}\right\rangle_\psi^{-1} \left\langle \frac{\mathbf{B}\cdot\nabla\theta}{N_z} B \frac{\partial}{\partial\theta}\left(\frac{\Pi_{\|,z}}{B}\right)\right\rangle_\psi$ increases in presence of such asymmetry of pressure anisotropy and is a direct effect of the vorticity source itself.

However, the term $\Gamma^{\nabla n_i} = \frac{I^2 T_i m_z \nu_{z,i}}{Ze^2} \frac{1}{L_{\psi,i}} \left(\left\langle \frac{N_z}{B^2}\right\rangle_\psi - \left\langle \frac{B^2}{N_z}\right\rangle_\psi^{-1} \right)$ also increases near the transport barrier thanks to the steepening of the temperature profile in the transport region. This effect,

called thermal screening, is an effect already observed in tokamaks [8] which prevent impurities from contaminating the core plasma.

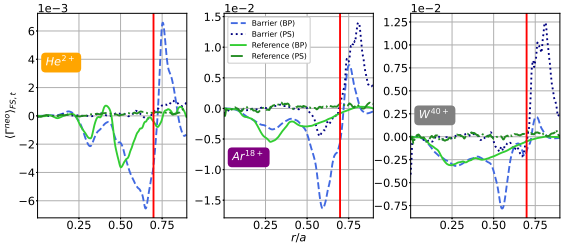

Figure 4: *Theoretical neoclassical particle flux-surface averaged fluxes for helium (left), argon (center) and tungsten (right). BP and PS fluxes for both the reference (solid light green and dotted-dashed lines for BP and PS fluxes respectively) and barrier (dashed light blue and dotted lines for BP and PS fluxes respectively) are presented separately. All profiles are time averaged over the last* $5000\omega_{c,i}^{-1}$ *of the simulations.*

The turbulent flux is, in presence of the transport barrier, severely reduced for all species as it has already been observed that the transport barrier quenches the turbulence intensity. A layer of negative flux is observed outside the barrier and can be linked to a local sign reversal of density (i.e. inward turbulent diffusion).

Conclusion

The transport barrier created through the vorticity source leads to increased neoclassical convection of particles on the inside of the barrier for all impurities. Particles cannot pass the transport barrier in one way or the other, increasing confinement on the inside of the barrier by isolating it from the outside. The barrier created through the vorticity source may be efficient in our simulations but may be unrealistic regarding the neoclassical transport (i.e. $\partial_\theta \Pi^{\parallel}$) and inward turbulent diffusion observed. The reduced turbulence in the core and thermal screening at the source location have however positive effects.

References

[1] K. Lim et al., Nucl. Fusion, vol. 61, no 4, p. 046037, 2021.

[2] V. Grandgirard et al., Comput. Phys. Commun., vol. 207, pp. 35–68, 2016.

[3] P. Guzdar et al., Phys. Fluids, vol. 26, no. 3, p. 673-677, 1983.

[4] A. Strugarek et al., Plasma Phys. Control. Fusion, vol. 55, no. 7, p. 074013, 2013.

[5] G. Lo-Cascio et al., Nucl. Fusion, vol. 62, no. 12, p. 126026, 2022.

[6] Angioni, C., Helander, P., Plasma Phys. Control. Fusion, vol. 56, no. 12, p. 124001, 2013.

[7] Donnel, P. et al., Plasma Phys. Control. Fusion, vol. 61, no 4, p. 044006, 2019.

[8] Field, A. et al., Nucl. Fusion, vol. 63, no 1, p. 016028, 2022.

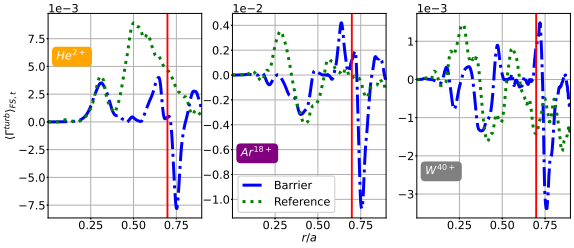

Figure 5: *Turbulent particle flux-surface averaged fluxes for helium (left), argon (center) and tungsten (right) in the reference (dotted green lines) and vorticity (dotted-dashed blue lines) cases. All profiles are time averaged over the last* $5000\omega_{c,i}^{-1}$ *of the simulations.*